## Investigation of Experimental Observables in Search of the Chiral Magnetic Effect in Heavy-ion Collisions in the STAR experiment

Fudan University, Shanghai, 200433 Lawrence Berkeley National Laboratory, Berkeley, California 94720 Abilene Christian University, Abilene, Texas 79699 Brookhaven National Laboratory, Upton, New York 11973 University of Tsukuba, Tsukuba, Ibaraki 305-8571, Japan Purdue University, West Lafayette, Indiana 47907 Southern Connecticut State University, New Haven, Connecticut 06515 State University of New York, Stony Brook, New York 11794 Rice University, Houston, Texas 77251 Physics Department and Center for Exploration of Energy and Matter, Indiana University, 2401 N Milo B. Sampson Lane, Bloomington, IN 47408, USA College of Physics and Technology, Guangxi Normal University, Guilin, 541004, China Central China Normal University, Wuhan, Hubei 430079, People's Republic of China Ohio State University, Columbus, Ohio 43210 University of Texas, Austin, Texas 78712 University of California, Los Angeles, California 90095 Department of Physics, McGill University, 3600 University Street, Montreal, QC, H3A 2T8, Canada Wayne State University, Detroit, Michigan 48201 Huzhou University, Huzhou, Zhejiang 313000

chiral

•

\_\_\_\_\_

in-plane out-of-plane

\_\_\_\_

— <sub>+</sub> — \_

<u>\sum\_+ \sum\_- \</u>

 $\sum$  +  $\sum$  +  $\sum$  -  $\sum$  -  $\sum$  -  $\sum$  + -

_	
	,
	√
[	] []

$$\sum$$

$$\left\langle \sum \right\rangle \\ \left\langle \sum \right\rangle \\ \sum \right\rangle \\ \frac{\alpha}{-*}$$

$$\int \left[ \int_{\alpha}^{*} - \int_{\alpha}^{*} - \int_{\alpha}^{*} - \int_{\alpha}^{*} - \right] -$$

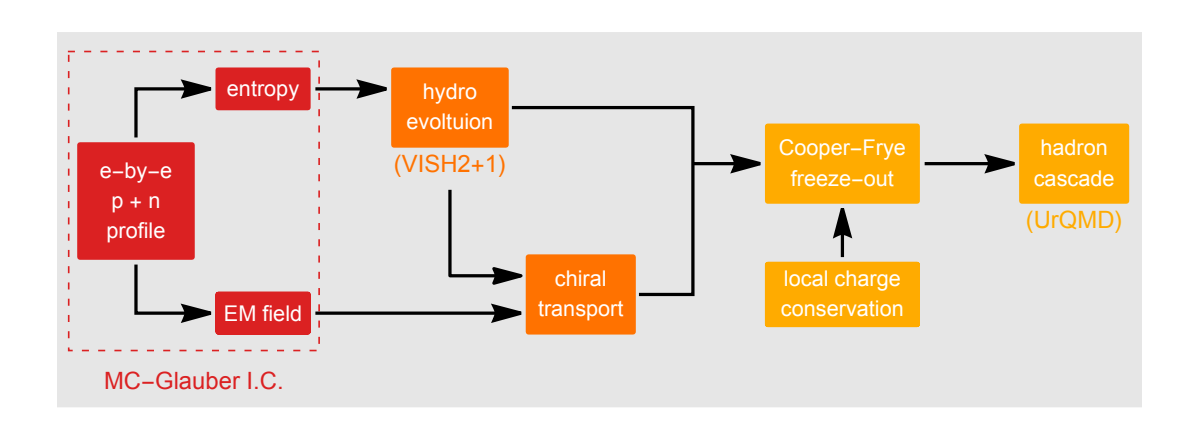
$$\int_{\alpha}^{\alpha} \left[ \int_{\alpha}^{\alpha} \int_{\alpha}^{\alpha}$$

\_

 ${\cal N}$   $_{T}$   $_{0}$   ${\cal N}$ 

extstyle ext

T = 
ho



s95p-v1.2

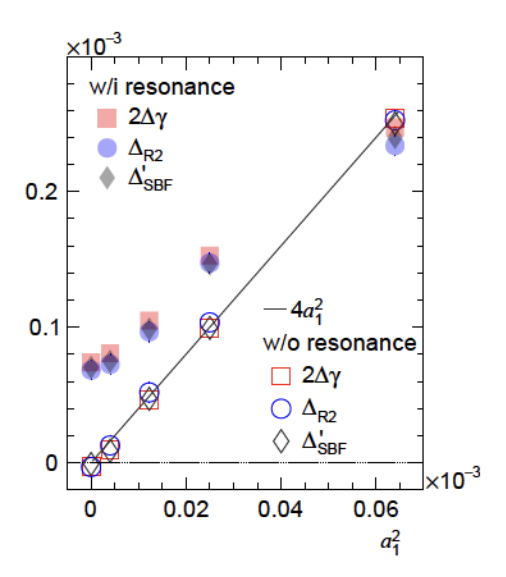


FIG. 2: The toy-model simulations of  $2\Delta\gamma_{112}$ ,  $\Delta_{R2}$  and  $\Delta'_{SBF} \equiv (\frac{\pi^4}{64M^2}\Delta_{SBF} + \frac{8}{3}v_2\Delta\delta)$  as function of the input  $a_1^2$ . The open markers represent the pure-signal scenario without resonances, and the solid markers denote the scenario with resonance decays. In comparison, the linear function of  $4a_1^2$  is also added.

and improved to mimic more realistically the impact of a finite charge-correlation length: a new parameter  $P_{\rm LCC}$  is introduced to characterize the fraction of charged hadrons that are sampled in positive-negative pairs in the same way as in Ref. [62], while the rest of the hadrons are sampled independently. Varying the parameter  $P_{\rm LCC}$  between 0 and 1 would tune the LCC contributions from none to its maximum. Finally, all the hadrons produced from the freeze-out hypersurface are further subject to hadron cascades through the UrQMD simulations [63], which account for various hadron resonance decay processes and automatically include their contributions to the charge-dependent correlations. The tuning of the EBE-AVFD calculations to the experimental measurements of  $\Delta\delta$  and  $\Delta\gamma_{112}$  in Au+Au collisions suggests that an optimal value of  $P_{\rm LCC}$  is around 1/3, and that roughly half of the background correlations come from LCC and the other half from resonance decays.

## IV. CORE-COMPONENT COMPARISONS

We will exploit the toy model and the EBE-AVFD model to simulate the core components of the experimental observables introduced in Sec. II:  $\Delta \gamma_{112}$  for the  $\gamma$  correlator,  $\Delta_{R2}$  for the R correlator, and  $\Delta_{\rm SBF}$  for the signed balance functions. Our objective is to examine the responses of the core components to the CME signal and the background, and to verify the relations between these methods (Eqs. 21 and 34). For a fair comparison with other observables, the momentum weighting is not applied in the  $\Delta_{\rm SBF}$  results. For simplicity, the true reaction plane is used in all the simulations in this section. The particles of interest are selected with  $|\eta| < 1$  and  $0.2 < p_T < 2$  GeV/c.

## A. Toy-model Results

We put the three core components on the same footing, by plotting  $2\Delta\gamma_{112}$ ,  $\Delta_{R2}$  and  $\Delta'_{SBF} \equiv (\frac{\pi^4}{64M^2}\Delta_{SBF} + \frac{8}{3}v_2\Delta\delta)$  as function of the input  $a_1^2$  in Fig. 2 for two scenarios: with and without resonance decays (LCC is not implemented in the toy model). In the background-free case without decays, the three observables render very similar results (open markers), all falling on the linear function of  $4a_1^2$ . Therefore, all the three methods are sensitive to the same amount of the CME signal. When resonance decays are turned on with finite elliptic flow, sizeable background effects appear besides the pure-signal contributions for all the three approaches (solid markers), more prominent at smaller input  $a_1^2$  values. Note that each final observable can be roughly regarded as a weighted average of the correlations due to the CME, the resonance background and the cross terms. At unrealistically large  $a_1^2$  values, the CME contribution in an observable could be diluted by the resonance contribution, since the latter becomes smaller than the former. The three core components exhibit similar responses to the backgrounds due to flowing resonances in this toy model. In this scenario, there are some subtle differences between the results from these three approaches, probably because of

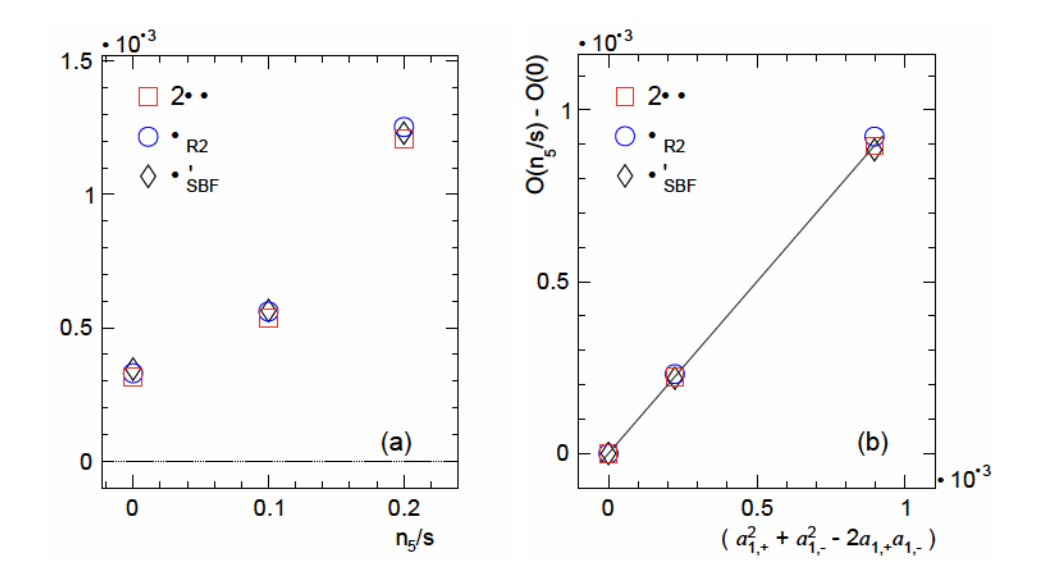


FIG. 3: (a) The EBE-AVFD simulations of  $2\Delta\gamma_{112}$ ,  $\Delta_{R2}$  and  $\Delta'_{\rm SBF} \equiv (\frac{\pi^4}{64M^2}\Delta_{\rm SBF} + \frac{8}{3}v_2\Delta\delta)$  as function of  $n_5/s$  in 30-40% Au+Au collisions at 200 GeV. (b) The same results with the subtraction of the pure-background case vs  $(a_{1,+}^2 + a_{1,-}^2 - 2a_{1,+}a_{1,-})$ . In comparison, a linear function of y = x is drawn to verify the relation in Eq. 39.

some higher-order effects omitted in the derivation of Eqs. 21 and 34. Although the background contributions depend on spectra and particularly elliptic flow of resonances [43, 44, 47], to the first order, we expect the three observables to have similar responses to resonance decays for a wide range of spectra or elliptic flow. A recent study [48] has also found that the R correlator and the  $\Delta\gamma_{112}$  correlator have similar sensitivities to the CME signal and the background.

## B. EBE-AVFD Results

The EBE-AVFD model implements the CME and the backgrounds in a more realistic way. In the following simulations, we generate the EBE-AVFD events of 30-40% Au+Au collisions at  $\sqrt{s_{\rm NN}} = 200$  GeV, with  $n_5/s = 0$ , 0.1 and 0.2. The background effects almost remain the same, whereas the CME signal is varied according to the input  $n_5/s$ . Figure 3(a) presents the corresponding calculations of  $2\Delta\gamma_{112}$ ,  $\Delta_{R2}$  and  $\Delta'_{\rm SBF}$  as function of  $n_5/s$ . The three methods yield very similar results at each input  $n_5/s$  value, supporting the relations expressed in Eqs. 21 and 34.

With the known reaction plane angle in each EBE-AVFD event, we can readily calculate  $a_{1,\pm}$ , and check if this CME contribution explains the difference between the cases with different  $n_5/s$  values.  $a_{1,\pm}$  is consistent with zero for  $n_5/s=0$ , and  $a_{1,+}$  and  $a_{1,-}$  are finite with opposite signs for finite  $n_5/s$  values. Note that  $a_{1,+}$  and  $a_{1,-}$  do not necessarily have the same magnitude, because the collision system always bears extra positive charges. Based on the expansion of the  $\gamma_{112}$  correlator in Eq. 3 and the equivalence between the three observables, we expect the following equation for any of these observables,  $O(n_5/s)$ ,

$$O(n_5/s) - O(0) = a_{1,+}^2 + a_{1,-}^2 - 2a_{1,+}a_{1,-}.$$
(39)

Figure 3(b) shows that the results for each observable, after the subtraction of the pure-background case, fall on the straight line representing the relation in Eq. 39. Thus, the EBE-AVFD calculations reveal the linear superposition of the CME signal and the background contribution in the experimental observables. This property is implicitly assumed by most of the analysis techniques that attempt to separate the CME signal and the backgrounds, and it is now corroborated by the EBE-AVFD model.

The core-component comparison using both the toy model and the EBE-AVFD model support the idea that to the first order, the three observables are equivalent to each other, with their very similar responses to the CME signal as well as the backgrounds.

		_		
		<u> </u>		
	<u> </u>	l		

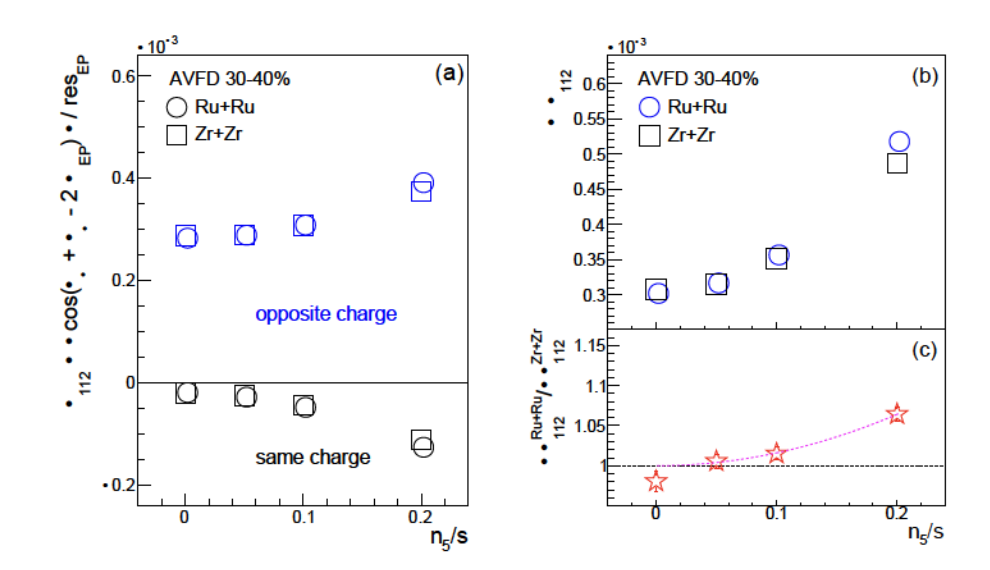


FIG. 4: EBE-AVFD calculations of  $\gamma_{112}^{\rm OS(SS)}$  (a) and  $\Delta\gamma_{112}$  (b) as functions of  $n_5/s$  for 30-40% isobaric collisions at  $\sqrt{s_{\rm NN}} = 200$  GeV, together with the ratio of  $\Delta\gamma_{112}$  (c) between Ru+Ru and Zr+Zr. In panel (c), the  $2^{\rm nd}$ -order-polynomial fit function illustrates the rising trend starting from (0, 1).

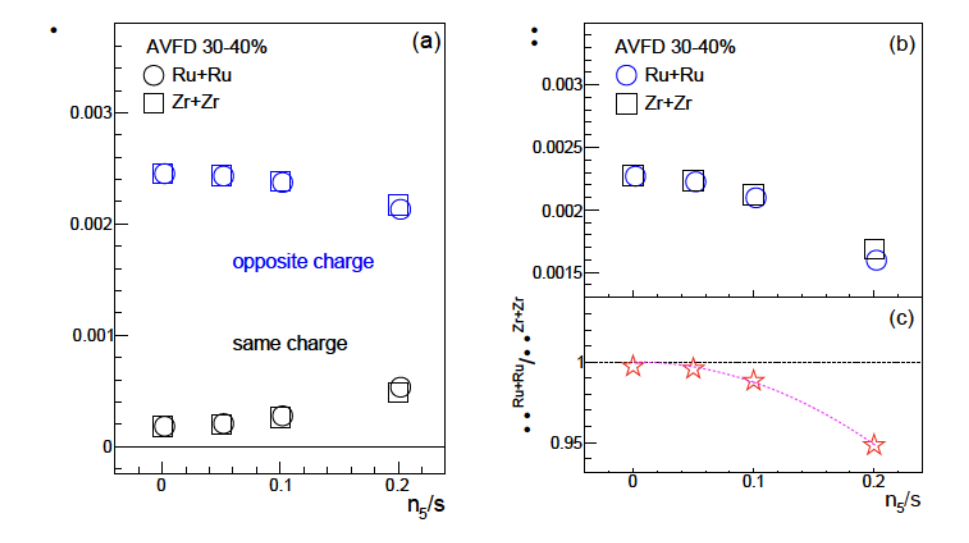


FIG. 5: EBE-AVFD calculations of  $\delta^{\rm OS(SS)}$  (a) and  $\Delta\delta$  (b) as functions of  $n_5/s$  for 30-40% isobaric collisions at  $\sqrt{s_{\rm NN}}=200$  GeV, together with the ratios of  $\Delta\delta$  (c) between Ru+Ru and Zr+Zr. In panels (c) , the 2<sup>nd</sup>-order-polynomial fit function is added to demonstrate the rising trend starting from (0, 1).

signal in  $\Delta\delta$  could be even larger than that in  $\Delta\gamma_{112}$  measured with respect to the participant plane [59]. This is because the magnetic field difference between the two isobaric systems is maximal with respect to the reaction plane, and is reduced when measured otherwise. The EBE-AVFD simulations indeed support this idea: at each  $n_5/s$  value in Fig. 5(c), the deviation of the  $\Delta\delta$  ratio from unity is at the similar level as that of the  $\Delta\gamma_{112}$  ratio. Since  $\Delta\delta$  is typically larger than  $\Delta\gamma$  by an order of magnitude, this similar deviation in their respective ratios indicates a significantly larger CME effect in  $\Delta\delta$  than in  $\Delta\gamma$ . A 2<sup>nd</sup>-order polynomial fit function is added to guide the eye. In view of the smaller relative statistical uncertainties of  $\Delta\delta$  than those of  $\Delta\gamma_{112}$ , the former may yield even better significance levels of the CME signal than the latter in the isobaric-collision data, provided equal background contributions to  $\Delta\delta$  in the two systems. The caveat is that the two-particle correlation background to  $\Delta\delta$  is significantly larger than that to  $\Delta\gamma$ , so any difference in the background between the two isobaric systems would have a stronger impact on  $\Delta\delta$ . However likely or unlikely this scenario is to occur, we keep these results for completeness and leave them to the test with

the real data. Between Ru+Ru and Zr+Zr, the difference in the background contributions to  $\Delta \gamma_{112}$  may be small, but could still be finite owing to the possibly different  $v_2$  values. The normalization of  $\Delta \gamma_{112}$  by  $v_2$  would be a more robust variable for the CME search.

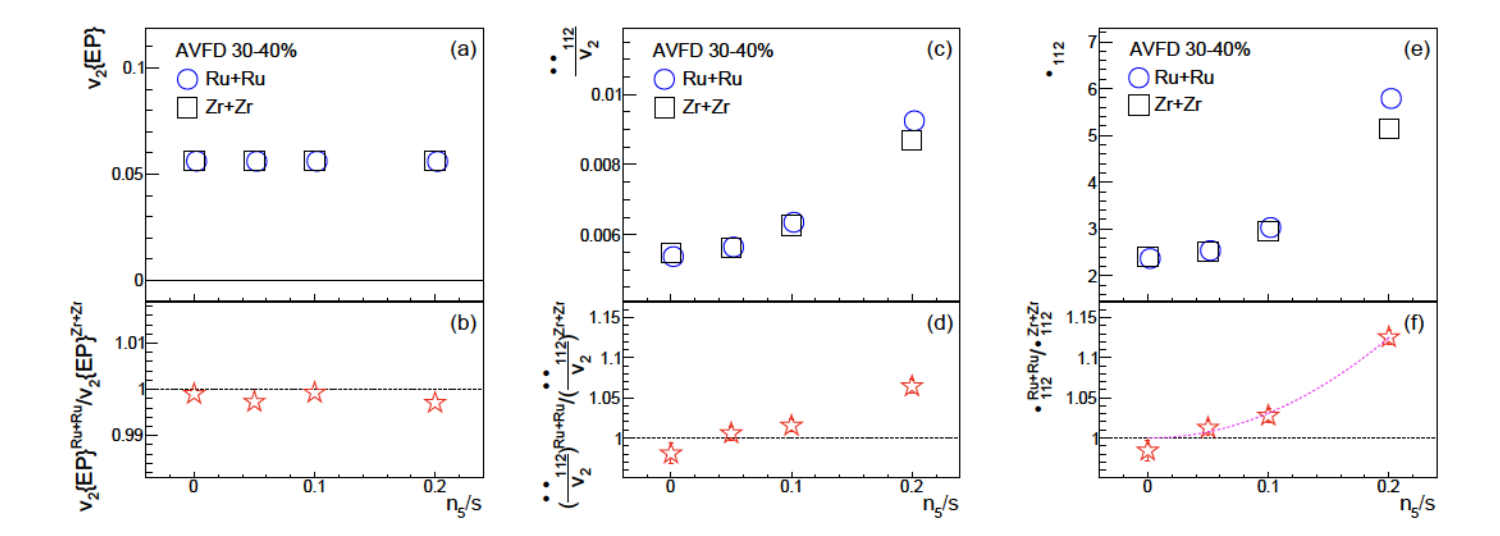


FIG. 6: EBE-AVFD calculations of  $v_2$  (a),  $\Delta \gamma_{112}/v_2$  (c) and  $\kappa_{112}$  (e) as functions of  $n_5/s$  for 30-40% isobaric collisions at  $\sqrt{s_{\rm NN}} = 200$  GeV, together with the ratios of  $v_2$  (b),  $\Delta \gamma_{112}/v_2$  (d) and  $\kappa_{112}$  (f) between Ru+Ru and Zr+Zr. In panels (f), the 2<sup>nd</sup>-order-polynomial fit function illustrates the rising trend starting from (0, 1).

The EBE-AVFD simulations of  $v_2$  (a) and  $\Delta\gamma_{112}/v_2$  (c) are presented in Fig. 6 as functions of  $n_5/s$  for 30-40% isobaric collisions at  $\sqrt{s_{\rm NN}}=200$  GeV, with the corresponding  $v_2$  ratio (b) and  $\Delta\gamma_{112}/v_2$  ratio (d) between Ru+Ru and Zr+Zr. The  $v_2$  values are very close to each other between Ru+Ru and Zr+Zr collisions, with the relative difference at the level of 0.1%. Because of this, the Ru+Ru/Zr+Zr ratio of  $\Delta\gamma_{112}/v_2$  in Fig. 6(d) is practically identical to that of  $\Delta\gamma$  in Fig. 4(c). Besides the possible  $v_2$  difference, the two-particle correlation strengths (which is part of the CME background) could also differ from Ru+Ru to Zr+Zr collisions. As we mentioned above, although  $\Delta\delta$  is also sensitive to the CME, it is overwhelmed by background correlations and thus may be used as an approximate gauge for the two-particle correlation strength. The additional normalization of  $\Delta\gamma_{112}/v_2$  by  $\Delta\delta$  in  $\kappa_{112}$  could, therefore, further suppress this difference, and enhance the sensitivity to the CME signal. There are two potential scenarios where  $\kappa_{112}$  has the advantage over  $\Delta\gamma_{112}$ . First, in reality the  $\Delta\delta$  ratio may disfavor the CME interpretation, and in that case, the  $\kappa_{112}$  ratio is less prone to a faked CME signal than the  $\gamma_{112}$  ratio. Second,  $\Delta\delta$  may also contain the CME signal as shown in Fig. 5(c), while the relative statistical uncertainty of  $\Delta\delta$  is smaller than that of  $\Delta\gamma_{112}^{Ru+Ru}/\kappa_{$ 

A similar frozen-code analysis is performed for the  $R(\Delta S_2)$  correlator, and the results are presented in Figure 7. In order to minimize the influence of the particle number fluctuations, the  $R(\Delta S_2)$  distribution is converted into the  $R(\Delta S_2')$  distribution by dividing the horizontal axis by the RMS of the  $N(\Delta S_{2,\text{shuffled}})$  distribution, i.e.,  $\Delta S_2' = \Delta S_2/\sqrt{\langle(\Delta S_{2,\text{shuffled}})^2\rangle}$ . Then  $\Delta S_2'$  is further modified to correct for the event plane resolution, i.e.,  $\Delta S'' = \Delta S'/\delta_{\text{Res}}$ , where  $\delta_{\text{Res}}$  is the correction factor whose details can be found in Ref. [54]. Panels (a) and (b) show the  $R(\Delta S_2'')$  distributions from EBE-AVFD events of 30-40% Ru+Ru and Zr+Zr collisions, respectively, at  $\sqrt{s_{\text{NN}}} = 200$  GeV with different  $n_5/s$  inputs. As  $n_5/s$  increases, the  $R(\Delta S_2'')$  distribution becomes more concave, qualitatively representing more CME contributions. To quantify the distribution shape, the Gaussian width  $(\sigma_{R2})$  is obtained by fitting each  $R(\Delta S_2'')$  distribution with an inverse Gaussian function, and the resultant  $\sigma_{R2}^{-1}$  values are listed in panel (c), increasing with  $n_5/s$ . The  $\sigma_{R2}^{-1}$  ratios between Ru+Ru and Zr+Zr are shown in panel (d). According to Eq. 22,  $\sigma_{R2}^{-1}$  is proportional to  $\sqrt{\Delta \gamma_{112}} \propto [(\sigma_{R2}^{-2})^{\text{CME}} + (\sigma_{R2}^{-2})^{\text{BG}}]^{1/2}$ , and hence the  $\sigma_{R2}^{-1}$  ratio is expected to follow a quadratic trend vs  $n_5/s$ ,

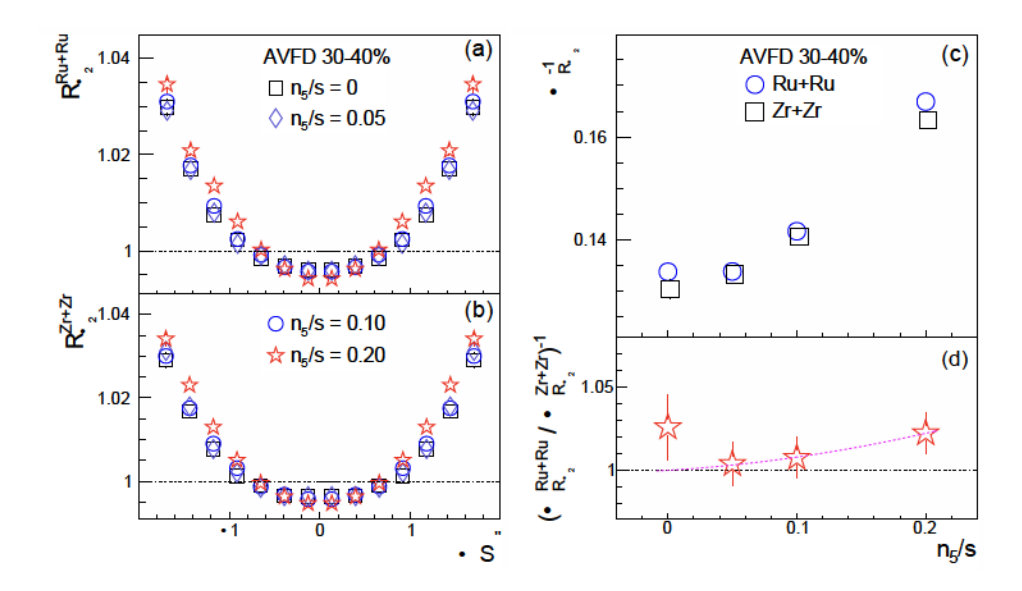


FIG. 7: Distributions of  $R(\Delta S_2'')$  from EBE-AVFD events of 30-40% Ru+Ru (a) and Zr+Zr (b) at 200 GeV with different  $n_5/s$  inputs. Panel (c) lists  $\sigma_{R2}^{-1}$  vs  $n_5/s$ , extracted from panels (a) and (b), and the  $\sigma_{R2}^{-1}$  ratios between Ru+Ru and Zr+Zr are shown in panel (d), where the 2<sup>nd</sup>-order-polynomial fit function shows the rising trend starting from (0, 1).

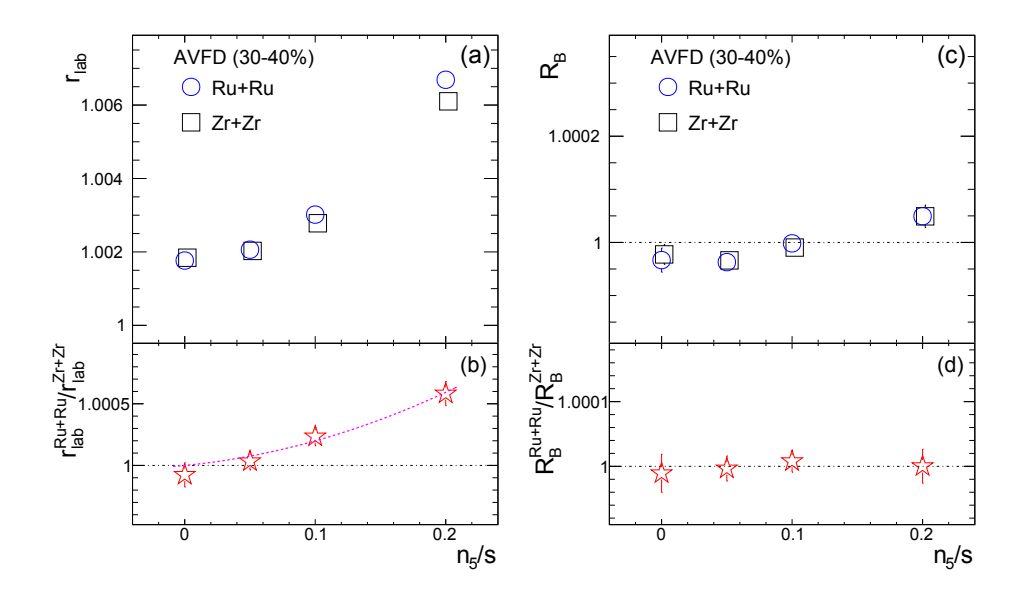
assuming the CME signal is small compared with the background. We fit the  $\sigma_{R2}^{-1}$  ratios with a 2<sup>nd</sup>-order polynomial function starting from (0, 1), though the statistical uncertainties are large. The significance values of these ratios are stored in Table II for later discussions.

Figure 8 presents the sensitivity study for the signed balance functions. This approach is not part of the STAR blind analysis, but follows the same procedure as used in the Quark Matter 2019 Conference proceedings [56]. The observables  $r_{\rm lab}$  and  $R_{\rm B}$  as defined in Eqs. 25 and 26 (with  $p_T$  weighting), respectively, are exhibited in panels (a) and (c) as function of  $n_5/s$  from the EBE-AVFD model for 30-40% Ru+Ru and Zr+Zr collisions at  $\sqrt{s_{\rm NN}}=200$  GeV. The corresponding ratios between Ru+Ru and Zr+Zr are shown in panels (b) and (d), respectively.  $r_{\rm lab}$  increases with the CME signal in each isobaric collision. According to Eqs. 25 and 34 and the core-component comparisons,  $r_{\rm lab}$  is related to  $\sqrt{\Delta\gamma_{112}}$ , and therefore the  $r_{\rm lab}$  ratio between the two systems should roughly obey a  $2^{\rm nd}$ -order polynomial function that starts from (0, 1). This relation is demonstrated with the corresponding fit in Fig. 8(b). Panel (d) does not show a clear trend for the ratio of  $R_{\rm B}^{\rm Ru+Ru}/R_{\rm B}^{\rm Zr+Zr}$ , which is not a complete surprise:  $R_B$  looks for a higher-order effect in the difference between  $r_{\rm lab}$  and  $r_{\rm rest}$ , and thus requires much more statistics than  $r_{\rm lab}$ . The sensitivity in terms of the statistical significance of  $(O^{\rm Ru+Ru}/O^{\rm Zr+Zr}-1)$  is listed in Table II for the observables,

The sensitivity in terms of the statistical significance of  $(O^{\text{Ru}+\text{Ru}}/O^{\text{Zr}+\text{Zr}}-1)$  is listed in Table II for the observables,  $\Delta\gamma_{112}$ ,  $\Delta\delta$ ,  $\kappa_{112}$ ,  $r_{\text{lab}}$  and  $\sigma_{R2}^{-1}$ . This table serves as a reference point to interpret the STAR data of the isobaric collisions. Note that opposite to other observables, the  $\Delta\delta$  ratio is supposed to be lower than unity in presence of the CME. Therefore, the more negative the statistical significance of  $(\Delta\delta^{\text{Ru}+\text{Ru}}/\Delta\delta^{\text{Zr}+\text{Zr}}-1)$ , the more sensitive this observable is to the CME signal. The high sensitivities of the  $\Delta\delta$  ratio reported in Table II could be a special feature of EBE-AVFD, instead of a universal truth, which awaits verification/falsification of real data. In general,  $\kappa_{112}$  roughly doubles the sensitivity of  $\Delta\gamma_{112}$ , which, as explained before, should be mostly due to the contribution of  $\Delta\delta$ , and needs to be tested by experimental data.

 $\Delta\gamma_{112}$  and  $r_{\rm lab}$  show similar significance values because of the approximate equivalence between them. Note that neither the toy model nor the EBE-AVFD model takes into account the separate CME domains that, instead of merging into a global charge separation for the whole event, still move independently from each other in the fireball. Thus  $r_{\rm lab}$  is expected by these models to respond to the CME signal in a similar way as  $\Delta\gamma_{112}$  that only deals with the azimuthal angle. Should the isobaric-collision data show a better sensitivity of  $r_{\rm lab}$  than that of  $\Delta\gamma_{112}$ , it may reveal the CME domains undergoing an incomplete hydrodynamic evolution due to its short duration.

In the analysis of the R correlator using the STAR frozen code,  $\sigma_{R2}^{-1}$  yields lower significance than other observables, and this is worth to note in anticipation of the results from the STAR blind analysis. However, this is largely due to two factors in this particular implementation. First, this analysis uses the sub event plane instead of the full event plane as



1			
	×		
	×		
	×		

```
\{\Sigma \} \{\Sigma \} \{\Sigma \}, \dots, n\}
\Sigma, \Sigma, \dots, n
\Sigma \Sigma, \dots, n
\Sigma, \Sigma \}
\langle \Sigma, \Sigma, \dots, n \rangle
\{\int \left[\int_{-\tilde{a}}^{\tilde{a}} - \int_{-\tilde{a}}^{\tilde{a}} - \right] - \int_{-\tilde{a}}^{\tilde{a}} - \left[-\int_{-\tilde{a}}^{\tilde{a}} - \right] - \left[-\int_{-\tilde{a}}^{\tilde{a}} - \int_{-\tilde{a}}^{\tilde{a}} - \left[-\int_{-\tilde{a}}^{\tilde{a}} - \int_{-\tilde{a}}^{\tilde{a}} - \right] - \left[-\int_{-\tilde{a}}^{\tilde{a}} - \int_{-\tilde{a}}^{\tilde{a}} - \left[-\int_{-\tilde{a}}^{\tilde{a}} - \left[-\int_{-\tilde{a}}^
```

$$\left\{ \sum \sum_{i=1}^{n} \left\{ \int_{i}^{n} \left[ \int_{i}^{n$$

 $egin{array}{l} et \ al. \\ et \ al. \\ et \ al. \\ et \ al. \end{array}$ 

 $\begin{array}{c} et \ al. \\ et \ al. \end{array}$ 

et~al.

et al. et al. et al. et al.

et~al.